

Synthesis and characterization of bioactive forsterite nanopowder

M. Kharaziha*, M.H. Fathi

Biomaterials Group, Department of Materials Engineering, Isfahan University of Technology, Isfahan, 84156-83111, Iran

Received 25 August 2008; received in revised form 27 December 2008; accepted 6 February 2009

Available online 25 February 2009

Abstract

Forsterite ceramic is a new bioceramic with good biocompatibility. However, the degradation rate of forsterite ceramic is extremely low, and the apatite-formation ability is also poor. On the other hand, nanostructured bioceramics are expected to have better bioactivity than coarser crystals. The aim of this work was preparation, characterization and bioactivity evaluation of forsterite nanopowder. Forsterite nanopowder was synthesized by the sol–gel process. Bioactivity evaluation was performed by immersing the forsterite powder in the simulated body fluid (SBF) and apatite formation on the surface of the immersed forsterite nanopowders was investigated. Results showed the particle size of pure forsterite was 25–45 nm. During immersion in SBF, the dissolution rate of the forsterite nanopowder was higher than conventional forsterite powders and apatite was formed after soaking for 14 days. Our study indicated that forsterite nanopowder unlike micron-sized forsterite possessed apatite-formation ability and might be used for preparation of new biomaterials.

© 2009 Elsevier Ltd and Techna Group S.r.l. All rights reserved.

Keywords: A. Sol–gel processes; D. Silicate; E. Biomedical applications; Nanopowder

1. Introduction

Bioactive ceramics have become one of the major fields in medicine over the last three decades. One remarkable success of bioactive ceramics is the clinical use of sintered hydroxyapatite (HA) for implants due to its bioactivity and osteoconductivity [1]. However, the low fracture toughness of HA ceramic ($0.6\text{--}1.0\text{ MPa m}^{1/2}$) limits the scope of clinical applications [2]. It is reported that compounds including SiO_2 , i.e., bioactive glasses [3], CaSiO_3 ceramics [4,5], apatite/Wollastonite (A/W) glass-ceramics [6] and dicalcium silicate [7] show good biocompatibility [8]. In recent years, some Si and Mg containing ceramics have drawn interests in the development of bone implant materials [9–12].

Forsterite (Mg_2SiO_4) is an important material in the magnesia–silica system [13]. Compared with hydroxyapatite ceramics, forsterite ceramics showed a significant improvement in the fracture toughness ($K_{\text{IC}} = 2.4\text{ MPa m}^{1/2}$) superior to the lower limit reported for bone implant [14]. In vitro studies showed significant osteoblast adhesion, spreading and growth

on the surface of forsterite ceramic [14]. Ni et al. [14,15] showed that forsterite ceramic is a novel bioceramic with high mechanical properties and good biocompatibility and might be suitable for hard tissue repair. However, the degradation rate of forsterite ceramic is extremely low, and the apatite-formation ability is also poor [15].

Motivated by the continuous need for orthopedic/dental implant formulations with improved osteointegrative (i.e., ability to bone to juxtaposed bone in situ) properties, Webster et al. [16–18] have previously designed, synthesized, and evaluated nanophase ceramic compacts with grain sizes less than 100 nm in diameter. Compared to respective conventional ceramic formulations, studies provided the first evidence of enhanced adhesion of osteoblasts (bone-forming cells), decreased adhesion of fibroblasts (cells that contribute to fibrous encapsulation and callus formation events that may lead to implant loosening and failure), and decreased adhesion of endothelial cells (cells that line the vasculature of the body) on nanophase alumina, titania, and hydroxyapatite [17].

Keeping the above points in view, forsterite nanopowder is expected to have better bioactivity than coarser crystals. Present study was aimed to produce and characterize synthetic forsterite nanopowder, and to evaluate the in vitro behavior of forsterite nanopowder in simulated body fluid.

* Corresponding author. Tel.: +98 311 3912750; fax: +98 311 3912752.

E-mail address: Kharaziha.ma@yahoo.com (M. Kharaziha).

2. Materials and methods

2.1. Preparation of forsterite (Mg_2SiO_4) nanopowder

Magnesium nitrate hexahydrate ($Mg(NO_3)_2 \cdot 6H_2O$, Merck, 99.99% purity), colloidal silica (SiO_2 , 34 wt.% solid fraction, Sigma), polyvinyl alcohol polymer (PVA) (Merck, molecular weight = 72,000), sucrose (Merck, 99.9% purity) and nitric acid were the starting materials. Fuel system combined PVA and sucrose (sucrose-to-metal molar ratio = 4:1) was applied to prepare forsterite. Water-based solutions of the magnesium salts and colloidal silica were prepared with the stoichiometric molar ratio of forsterite ($Mg:Si = 2:1$ mol) by pouring colloidal silica into the aqueous solution of magnesium nitrate (0.0142 mol magnesium nitrate) dissolved in 50 cc deionised water. The aqueous solution of sucrose (sucrose-to-metal ratio = 4:1 mol) in 100 cc deionised water was added dropwise to the precursor solution and the two solutions were homogenized together on a warming plate under 2 h continuous stirring. PVA (PVA monomer-to-metal molar ratio = 0.8:1) dissolved by 20 cc deionized water was added in to the final solution and the pH value was adjusted to 1 using nitric acid and the solution was mixed homogeneously by constant stirring for 2 h with a magnetic stirrer. Subsequent heating at 80 °C for 2 h on a hot plate stirrer the prepared gel was aged for 24 h. The prepared gel was then heated on a hot plate at 100 °C in air for enough time for complete dehydration and changing into a voluminous, black, fluffy gel. Finally, the dried gel was calcined in a furnace at 800 °C for 2 h.

2.2. Characterization of forsterite (Mg_2SiO_4) nanopowder

Phase structure analyses of obtained powders were carried out by X-ray diffractometer (XRD, Philips Xpert) using Ni filtered $Cu K\alpha$ ($\lambda_{Cu K\alpha} = 0.154$ nm, radiation at 40 kV and 30 mA) over the 2θ range of 20–80° (time per step: 1.25 s and step size: 0.05°). The obtained experimental patterns were compared to standards compiled by the Joint Committee on Powder Diffraction and Standards (JCDPS) [19]. The crystallite size of the forsterite nanopowders were determined by using the Scherrer equation (Eq. (1)):

$$\beta = \frac{K\lambda}{t \cos \theta} \quad (1)$$

where β is the width of peak in the middle of its height, λ is the wavelength (=0.154 nm), θ is the Bragg angle, k is a constant (=0.9), and t is the apparent crystallite size. For this purpose, three diffraction peaks (2 1 1), (2 2 2), and (4 0 0), which have the advantage of being well separated and which have high intensities, were chosen for the measurement. The half-widths were calculated by sigma plot software. Transmission electron microscopy (TEM; Leo 912AB) technique was utilized to characterize the morphology and nanostructure of the synthesized forsterite powder.

2.3. In vitro bioactivity evaluation

In vitro bioactivity of the obtained powders was investigated by soaking prepared forsterite nanopowder in the simulated body fluid (SBF) for 1, 7, 14, 21 and 28 days at a solid/liquid ratio of 1.5 mg/ml without refreshing the soaking medium. This procedure has been widely used to prove the similarity between in vitro and in vivo behavior of certain bioceramic compositions. The SBF was prepared according to the procedure described by Kokubo and Takadama [20]. The soaking experiment was carried out in a shaking bath maintained at 37 °C. After the preselected soaking time, the powders were filtrated and gently rinsed with deionized water to remove SBF solutions followed by drying at 100 °C. The apatite formation on the surface of the samples as a consequence of the dissolution and precipitation process of calcium phosphate was investigated by Fourier transitioned-infrared spectroscopy (FTIR; Bomem, MB 100) (The spectrum was recorded in the 4000–400 cm^{-1} region with 2 cm^{-1} resolution), X-ray diffractometer (XRD, Philips Xpert), scanning electron microscopy (SEM; S360, Cambridge) and energy dispersive X-ray (EDX). The concentrations of Ca and Mg of the SBF solutions after soaking were determined by atomic absorption spectrometer (AAS) (3030), The concentrations of P of the SBF solutions after soaking were determined by spectrophotometer (6505, Genway) and the changes in pH of soaking solutions were also measured at pre-determined time intervals (0–28 days) using an electrolyte-type pH meter.

3. Results and discussion

3.1. Characterization and phase structure analysis

Fig. 1 illustrates X-ray diffraction patterns of calcined gel of forsterite powder at 800 °C. Pure forsterite was formed at 800 °C. The crystallite size of forsterite at this temperature is in the range of 17–20 nm according to the XRD line-broadening technique and using the Scherrer equation. Saberi and Alinejad [21] synthesized nanocrystalline forsterite by this method after calcination for 3 h at 800 °C with crystal size in the range of 12–30 nm.

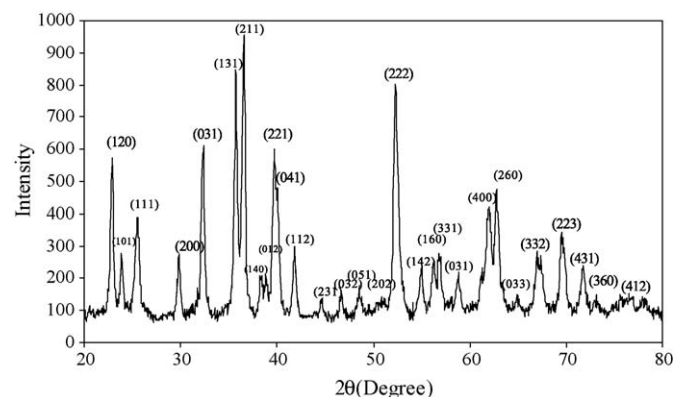


Fig. 1. X-ray diffraction patterns of forsterite powder calcined at 800 °C.

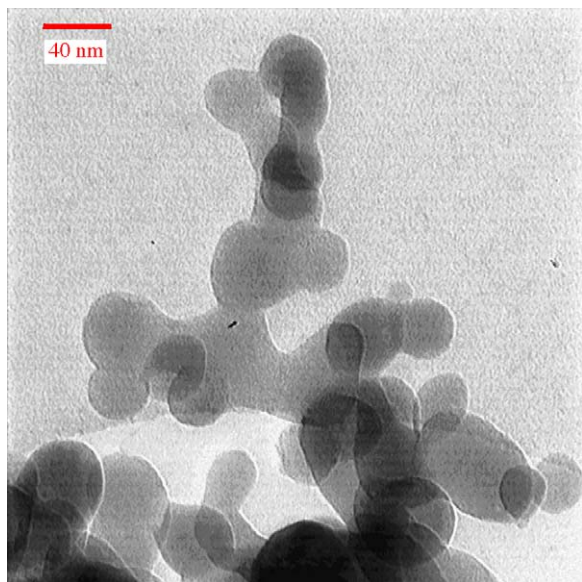


Fig. 2. TEM micrograph of forsterite nanopowders calcined at 800 °C.

The morphological shape and size of forsterite powder is shown in Fig. 2. Uniform sized particles with spherical shape are formed by this process. The average particle size of the forsterite powders measured from TEM was 25–45 nm.

3.2. *In vitro* bioactivity evaluation of forsterite nanopowder

The FTIR spectra of the forsterite nanopowder before and after soaking in the SBF are shown in Fig. 3. Before immersing in the SBF, the bands related to the characteristic peaks of forsterite appear in the range of 830–1000 cm^{-1} (SiO_4 stretching), at 500–620 cm^{-1} (SiO_4 bending) and at 475 cm^{-1} for modes of octahedral MgO_6 are shown. By soaking in the SBF, the intensity of silicate absorption bands decreased. Simultaneously, new absorption bands at 471 cm^{-1} and 574 cm^{-1} could be recognized after 2 week of soaking, which were split from the P–O bending vibration in a PO_4 tetrahedron around 598 cm^{-1} . The P–O stretching vibration of the PO_4 unit occurs at range 1030–1090 cm^{-1} . As this is superimposed with the strong vibration of the Si–O bond in SiO_4 unit, it is difficult to distinguish the P–O vibration from the Si–O vibration at the early stage of the reaction.

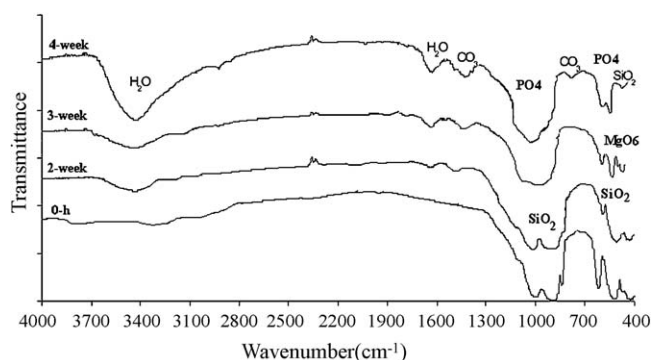


Fig. 3. FTIR spectra of forsterite nanopowders soaked in SBF solutions for various periods.

According to the report of infrared correlation charts [22], the bands at 574 cm^{-1} , 1030–1090 cm^{-1} and 471 cm^{-1} were all the characteristic of apatite crystals, which suggest the formation of apatite on the surface layer of Mg_2SiO_4 powders after soaking in SBF. Furthermore, the C–O stretching of CO_3^{2-} groups at 1418 cm^{-1} and 1462 cm^{-1} were observed, and the C–O stretching of CO_3^{2-} groups at 872 cm^{-1} appeared after soaking for 2 weeks. The bands assigned to the hydroxyl groups (OH) in the hydroxyapatite (3477 cm^{-1} and 1619 cm^{-1}) can be clearly observed in the spectra [22].

3.3. Microstructure of the formed apatite

The surface morphology and EDX spectra of the forsterite nanopowder after immersion in the SBF solution for 14 and 28 days are depicted in Fig. 4. After 14-day soaking, tiny ball-like particles with crystallites sizes in about 400–500 nm in diameter were observed on the surface of powders. The EDX spectrum indicates that the tiny ball-like particles are composed of calcium and phosphorus but Mg and Si in the EDX spectrum originate from the forsterite. After prolonged soaking for up to 28 days, clusters of agglomerated HAp particles increased and the surface structure of the samples became more compact. The EDX spectrum indicates that the granules are composed of mainly calcium and phosphorus. (The Au in the EDX spectrum originates from the coating.) Studies on the other ceramics such as tricalcium silicate ceramics showed the same morphology of the apatite (tiny ball-like particles) in the low magnification. The higher magnification SEM micrograph showed that the particles of apatite were lathlike and the size of the particles was about 50 nm in diameter [23,24].

Fig. 5 shows the XRD patterns of forsterite nanopowder before and after soaking in the SBF solution. Although the characteristic peaks of forsterite can be seen, the characteristic peaks for apatite became the main constituent of the XRD patterns as the HAp content covered the surfaces of the powders after soaking for 28 days. XRD pattern proved that apatite could fabricate on the forsterite nanopowder surface by immersing in the SBF.

3.4. Changes of pH and ion concentrations of the SBF

Fig. 6 shows changes of the pH and the concentrations of Ca, P and Mg of SBF solutions after soaking for various periods of time. It is obvious that the ion concentrations of SBF solutions changed after 1 day of soaking. The Mg concentrations in SBF increased while P and Ca concentration gradually decreased at the early stage of soaking (Ca concentration decreased from 2.5 mM to 1.78 mM and P concentration decreased from 1 mM to 0.55 mM, only after 1 day soaking in the SBF). The Ca and P concentrations continued to decrease in solutions due to a consumption of these ions during the subsequent formation of apatite on the surface of the powders. The Ca and P concentrations in the SBF solution decreased steeply with a corresponding increase in the Mg concentration. This reflected the dissolution of the Mg accompanied with simultaneous uptake of Ca and P from the solution onto the paste, which

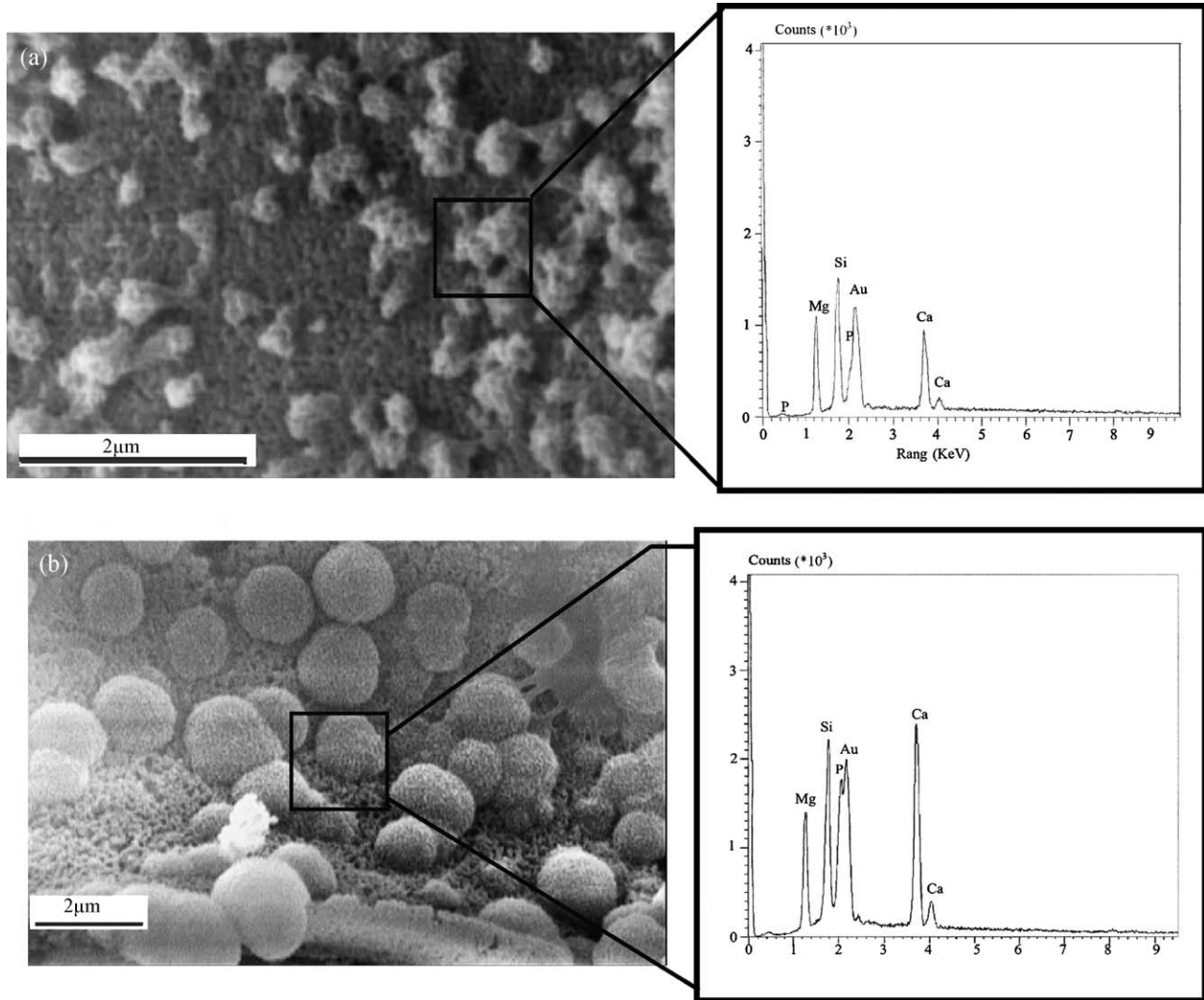


Fig. 4. SEM photograph and EDX spectrum of the forsterite nanopowders after immersion in SBF solution for (a) 14 days and (b) 28 days.

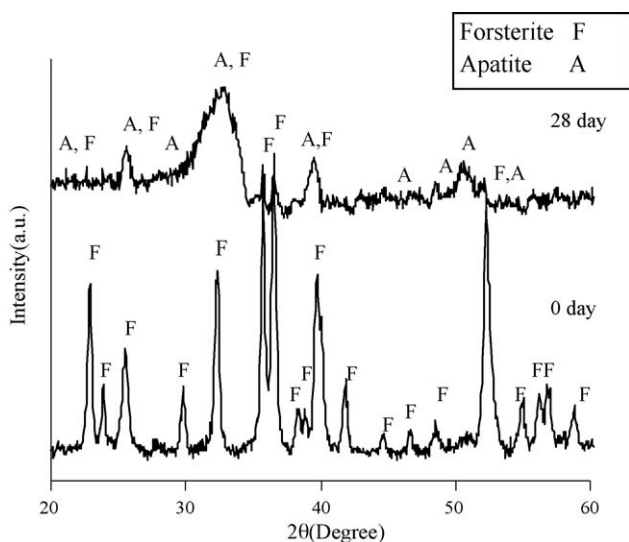


Fig. 5. XRD patterns of the forsterite nanopowder before and after 28 days soaking in SBF.

corresponded to a quick increase of the pH value of the SBF solution reached a maximum in the 7 days, and then decreased gradually due to consuming OH^- ions in the formation of HAp.

The pH value is dependent on the solubility or resorbability of the forsterite nanopowder. According to Fig. 6, the prepared forsterite nanopowder has bioresorption which can be attributed to its high surface area to volume ratio owing to nanostructure processing. The magnesium ions release of prepared forsterite nanopowders into SBF medium was quantitatively estimated to support its in vitro bioresorbability (Fig. 6).

In this study, our results indicate that forsterite nanopowder possess apatite-formation ability and is bioactive. Furthermore, the profile of the changes of Ca, Mg and P ion concentrations and pH in SBF is similar to that of the $\text{CaO-SiO}_2\text{-MgO}$ based bioactive ceramics (such as bredigite) [25]. Thus, the mechanism of apatite formation on the forsterite nanopowder might be similar to that of the $\text{CaO-SiO}_2\text{-MgO}$ based bioactive ceramics. When the forsterite nanopowder is immersed in the SBF, magnesium ions in the powder first exchange with H^+ in the solution led to the formation of silanol (Si-OH^-) in the

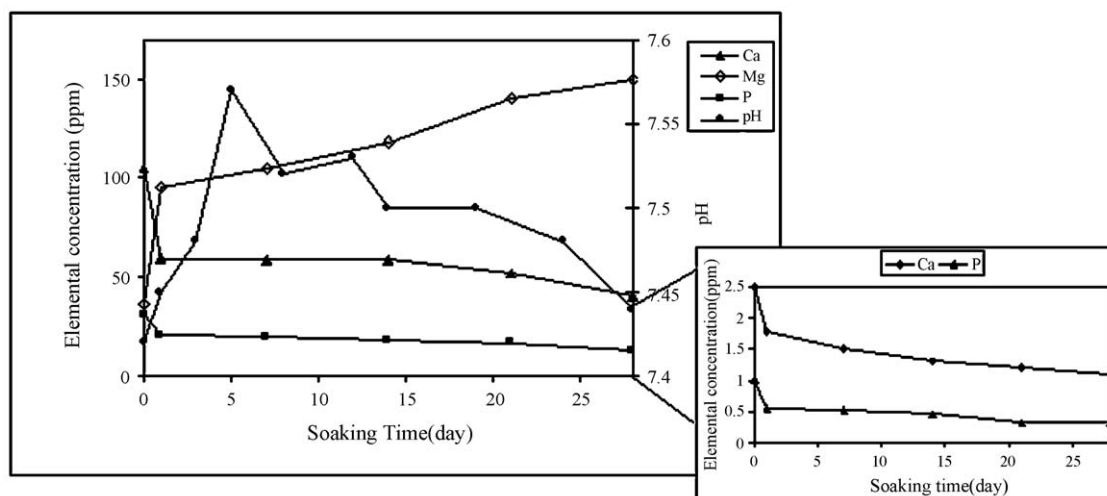


Fig. 6. Changes of Ca, Mg, and P concentrations, and pH of the SBF solution after soaking the forsterite nanopowders for various periods.

surface layer, a pH increase, and finally the production of a negatively charged surface with the functional group (Si-OH^-). The Ca ions in the SBF solution are initially attracted to the interface between the powder and solution. A result of calcium accumulating on the silica-rich layer is diminishing of phosphorus concentration in the SBF. Presence of enough calcium and phosphorus on the forsterite nanopowder cause formation of calcium-phosphate layer on the surface of forsterite nanopowder.

The bioactivity of an artificial material can be evaluated by examining the formation of apatite on its surface in SBF. Representative bioactive ceramics are Bioglass, HA, and glass-ceramic A/W, contain HA or its components, such as CaO and P_2O_5 . Therefore, it had been believed that a material should have these components for it to have apatite-forming ability and for it to be able to integrate with bone in the body. However, assessments of apatite formation on materials with different compositions in SBF imply that CaO and P_2O_5 in the composition of ceramics are not the essential components for apatite formation. Other composition such as glasses in the systems: $\text{CaO-P}_2\text{O}_5\text{-SiO}_2$ [26], $\text{Na}_2\text{O-CaO-SiO}_2$ [27], and $\text{K}_2\text{O-SiO}_2\text{-TiO}_2$ [28] can form apatite in the SBF solution. Interestingly, in the $\text{CaO-P}_2\text{O}_5\text{-SiO}_2$ system, the composition of the glass forming an apatite layer in an SBF was based on the CaO-SiO_2 system and not on the $\text{CaO-P}_2\text{O}_5$ system. The P_2O_5 -free CaO-SiO_2 glasses were actually shown to bond to living bone in animals by forming apatite on their surfaces [29]. Evaluation of the $\text{Na}_2\text{O-CaO-SiO}_2$ system indicates that, not only the P_2O_5 -free CaO-SiO_2 glasses, but also the CaO- and P_2O_5 -free $\text{Na}_2\text{O-SiO}_2$ glasses can form apatite in SBF.

Results of the present study indicated that forsterite nanopowder unlike micron-sized forsterite, possessed calcium phosphate layer formation ability and is bioactive. Similar results were obtained about calcium phosphate ceramic [30,31], which shows that the in vitro and in vivo Ca^{2+} ion release from the synthetic HA nanopowders are similar to bone apatite and significantly faster than microscale conventional HA. The powders dissolution rate is dependent largely to the crystallinity

level, phase composition, microstructure, surface area and density. The nanometer-sized grains and the high-volume fraction of grain boundaries in nanostructured materials have been found to increase osteoblast adhesion, proliferation, osteointegration, and the deposition of calcium containing minerals on the surface of these materials [17].

4. Conclusion

Forsterite nanopowder with particle size in the range of 25–45 nm was prepared using an amorphous polymeric precursor of sucrose and polyvinyl alcohol polymer molecules with the metal cations. The in vitro bioactivity test shows that forsterite nanopowder, unlike large particle-sized forsterite, was bioactive, which can be attributed to its high surface area owing to nanostructure processing. Our results indicate that forsterite nanopowder possess good in vitro bioactivity and biocompatibility, and may be used as bioactive bone repair materials. However, further in vivo studies need to be conducted to explore the applicability of these ceramics as implant materials. The profile of the changes of ions concentrations and pH in SBF was similar to that of the $\text{CaO-SiO}_2\text{-MgO}$ based bioactive ceramics. All these results suggested that the mechanism of HAp formation on the forsterite nanopowder might be similar to that of the $\text{CaO-SiO}_2\text{-MgO}$ based bioactive ceramics.

Acknowledgement

The authors are grateful for support of this research by Isfahan University of Technology.

References

- [1] H. Ohgushi, V.M. Goldberg, A.I. Caplan, Heterotopic osteogenesis in porous ceramics induced by marrow cells, *J. Orthop. Res.* 7 (1989) 568–578.
- [2] W. Suchanek, M. Yoshimura, Processing and properties of hydroxyapatite-based biomaterials for use as hard tissue replacement implants, *J. Mater. Res.* 13 (1998) 94–117.

- [3] I. Izquierdo-Barba, A.J. Salinas, M. Vallet-Reg, Effect of the continuous solution exchange on the in vitro reactivity of a CaO–SiO₂ sol–gel glass, *J. Biomed. Mater. Res.* 51 (2000) 191–199.
- [4] K. Lin, W. Zhai, S. Ni, J. Chang, Y. Zeng, W. Qian, Study of the mechanical property and in vitro biocompatibility of CaSiO₃ ceramics, *Ceram. Int.* 31 (2005) 323–326.
- [5] A. Binnaz Yoruc, Hazar, Preparation and in vitro bioactivity of CaSiO₃ powders, *Ceram. Int.* 33 (2007) 687–692.
- [6] S. Yoshii, Y. Kakutani, T. Nakamura, T. Kitsugi, M. Oka, T. Kokubo, Strength of bonding between A-W glass ceramic and the surface of bone cortex, *J. Biomed. Mater. Res.* 22 (A) (1988) 327–332.
- [7] Z. Gou, J. Chang, W. Zhai, Preparation and characterization of novel bioactive dicalcium silicate ceramics, *J. Eur. Ceram. Soc.* 25 (2005) 1507–1514.
- [8] G. Muralithran, S. Ramesh, The effects of sintering temperature on the properties of hydroxyapatite, *Ceram. Int.* 26 (2000) 221–230.
- [9] C.C. Mardare, A.I. Mardare, J.R.F. Fernandes, R.N. Correia, Deposition of bioactive glass-ceramic thin-films by RF magnetron sputtering, *J. Eur. Ceram. Soc.* 23 (2003) 1027–1030.
- [10] S.R. Kim, J.H. Lee, Y.T. Kim, D.H. Riu, S.J. Jung, Y.J. Lee, S.C. Chung, Y.H. Kim, Synthesis of Si, and Mg substituted hydroxyapatites and their sintering behaviors, *Biomaterials* 24 (2003) 1389–1398.
- [11] T.J. Webster, E.A. Massa-Schlueter, J.L. Smith, E.B. Slamovich, Osteoblast response to hydroxyapatite doped with doped with divalent and trivalent cations, *Biomaterials* 25 (2004) 2111–2121.
- [12] C.T. Wu, J. Chang, Synthesis and apatite-formation ability of akermanite, *Mater. Lett.* 58 (2004) 2415–2417.
- [13] M.H. Fathi, M. Kharaziha, Mechanically activated crystallization of phase pure nanocrystalline forsterite powders, *Mater. Lett.* 62 (2008) 4306–4309.
- [14] S. Ni, L. Chou, J. Chang, Preparation and characterization of forsterite (Mg₂SiO₄) bioceramics, *Ceram. Int.* 33 (2007) 83–88.
- [15] S. Ni, L. Chou, J. Chang, In vitro studies of novel CaO–SiO₂–MgO system composite bioceramics, *J. Mater. Sci.: Mater. Med.* 19 (2008) 359–367.
- [16] T.J. Webster, R.W. Siegel, R. Bizios, Design and evaluation of nanophase alumina for orthopedic/dental applications, *Nanostruct. Mater.* 12 (1999) 983–986.
- [17] T.J. Webster, R.W. Siegel, R. Bizios, Osteoblast adhesion on nanophase ceramics, *Biomaterials* 20 (1999) 1221–1227.
- [18] T.J. Webster, C. Ergun, R.H. Doremus, R.W. Siegel, R. Bizios, Specific proteins mediate enhanced osteoblast adhesion on nanophase ceramics, *J. Biomed. Mater. Res.* 51 (3) (2000) 475–483.
- [19] JCPDS Card No. 34-0189, 1984.
- [20] T. Kokubo, H. Takadama, How useful is SBF in predicting in vivo bone bioactivity, *Biomaterials* 27 (2006) 2907–2915.
- [21] A. Saberi, B. Alinejad, A novel method to low temperature synthesis of nanocrystalline forsterite, *Mater. Res. Bull.* 42 (2007) 666–673.
- [22] B.O. Fowler, Vibrational assignments for calcium, strontium, and barium hydroxyapatites utilizing isotopic substitution, *Inorg. Chem.* 13 (1974) 194.
- [23] W. Zhao, J. Wang, W. Zhai, Z. Wang, J. Chang, The self-setting properties and in vitro bioactivity of tricalcium silicate, *Biomaterials* 26 (2005) 6113–6121.
- [24] W. Zhao, J. Chang, J. Wang, W. Zhai, Z. Wang, In vitro bioactivity of novel tricalcium silicate ceramics, *J. Mater. Sci.: Mater. Med.* 18 (2007) 917–923.
- [25] C. Wu, J. Chang, J. Wang, S. Ni, W. Zhai, Preparation and characteristics of a calcium magnesium silicate (bredigite) bioactive ceramic, *Biomaterials* 26 (2005) 2925–2931.
- [26] C. Ohtsuki, T. Kokubo, K. Takatsuka, T. Yamamuro, Compositional dependence of bioactivity of glasses in the system CaO–SiO₂–P₂O₅: its in vitro evaluation, *J. Ceram. Soc.* 99 (1991) 1–6.
- [27] H.M. Kim, F. Miyaji, T. Kokubo, C. Ohtsuki, T. Nakamura, Bioactivity of Na₂O–CaO–SiO₂ glasses, *J. Am. Ceram. Soc.* 78 (1995) 2405–2411.
- [28] H.M. Kim, F. Miyaji, T. Kokubo, M. Kobayashi, T. Nakamura, Bioactivity of M₂O–TiO₂–SiO₂ (M = Na, K) glasses: an in vitro evaluation, *Bull. Chem. Soc.* 69 (1996) 2387–2394.
- [29] K. Ohura, T. Yamamuro, T. Nakamura, T. Kokubo, Y. Ebisawa, Y. Kotoura, M. Oka, Bone-bonding ability of P₂O₅-free CaO–SiO₂ glasses, *J. Biomed. Mater. Res.* 25 (1991) 357–365.
- [30] D.L. Wise, D.J. Trantolo, L. Kai-Uwe, J.D. Gresser, M.V. Cattaneo, M.J. Yaszemski, *Biomaterials Engineering and Devices: Human Applications, Orthopedic, Dental and Bone Graft Applications*, vol. 2, Humana Press, Totowa, NJ, 2000.
- [31] R. Murugan, S. Ramakrishna, Coupling of therapeutic molecules onto surface modified coralline hydroxyapatite, *Biomaterials* 25 (2004) 3073–3080.